Novel Hydrothermal Synthesis of CoS_2/MWCNT Nanohybrid Electrode for Supercapacitor: A Systematic Investigation on the Influence of MWCNT

Novel Hydrothermal Synthesis of CoS_2/MWCNT Nanohybrid Electrode for Supercapacitor: A Systematic Investigation on the Influence of MWCNT

A. Sarkar [a,b], Amit K. Chakraborty [a,c,], S. Bera [a,b], and S. Krishnamurthy [d]*

[a]Centre of Excellence in Advanced Materials, National Institute of Technology, Durgapur-713209, WB, India

[b]Department of Metallurgical and Materials Engineering, National Institute of Technology, Durgapur-713209, WB, India

[c]Carbon Nanotechnology Laboratory, Department of Physics, National Institute of Technology, Durgapur-713209, WB, India

[d]Department of Engineering and Innovation, The Open University, Milton Keynes, MK 76AA, U.K.

Abstract: Here we report a novel hydrothermal method to synthesize hybrid nanostructures based on single phase cobalt disulphide (CoS_2) nanoparticles decorated on multiwalled carbon nanotubes (MWCNT) for application as supercapacitor electrode. This is also the first report on systematic investigation of the influence of MWCNTs on the electrochemical properties of CoS_2 nanoparticle based electrode for supercapacitor. The X-ray diffraction and electron microscopic analyses revealed that incorporation of CNTs promote the growth of only CoS_2 phase in the form of spherical nanoparticles with an average diameter of ~9 nm. CoS_2-MWCNT nanohybrid electrode containing 20 wt% MWCNT showed the highest specific capacitance of 1486 F/gm at 1 A/gm discharge current density along with excellent reversibility. It also showed high cycle stability with ~80% retention of specific capacitance even after 10,000 cycles. Thus we show a low cost and simple method to synthesize a CoS_2-MWCNT nanohybrid that has great promise as electrode material for supercapacitor applications. Incorporation of CNT not only provides with a conducting network for fast charge diffusion but (due to large surface area) also allows more CoS_2 molecules to be readily available for redox reaction resulting in the reduction of the charge transfer resistance consistent with the data obtained from electrochemical impedance spectroscopy.

*Corresponding author Tel. +91 343 275 4780, Email: *amit.chakraborty@phy.nitdgp.ac.in* (Amit K. Chakraborty)

1. Introduction

Environmental changes and depletion of conventional energy sources have lead the researchers towards alternative renewable energy sources to meet the high prerequisites of future applications. Supercapacitors, also known as electrochemical capacitors or ultracapacitors, have attracted immense interest in automobile and electronics industry because of their high energy and power densities along with long cycle life.[1–4] Supercapacitors can be classified into two categories, pseudocapacitors and electric double layer capacitors (EDLCs). In pseudocapacitors, charge storage happens by faradaic reduction-oxidation reactions (redox reactions), and intercalation processes and usually exhibit higher capacitance values than those of EDLCs in which case the electrostatic storage of the electrical energy is achieved by separation of the charges in a Helmholtz double layer at the interface between the surface of a conductor electrode and an electrolyte.[3] Various metal oxides (MnO_2, Fe_2O_3, Co_3O_4), and conducting polymers (polyaniline, polypyrrole) are generally utilized as the cathode material in pseudocapacitors,[5–9]whereas carbon based nanostructures (carbon nanotube (CNT), graphene, etc.) are used in EDLC.[3–10] Metal oxides have good electrocatalytic properties but suffer from poor electrical conductivity which restricts their performance as electrode.[5–7]Conducting polymers despite good redox properties suffer from slow ion diffusion rate, poor chemical and thermal stability leading to low cycle-life.[8–9] On the other hand, in spite of excellent electrical conductivity, superior mechanical and chemical stability of CNT and graphene [11–12] poor specific capacitance restricts their use as supercapacitor electrode.

Therefore, in order to design novel electrodes with fast charge transport property, high electrocatalytic activity and long cycle life, often two or more of these three groups of materials are combined to form hybrid nanocomposites.[13–19] Transition metal sulphides and in particular, cobalt sulphide (CoS, CoS_2, Co_9S_8 etc.) have also been reported recently as a good pseudocapacitive material for supercapacitor electrode application.[20–22]However, poor electrical conductivity and tendency to agglomeration are the main hindrance for their application as electrodes which can be overcome by incorporation of carbon materials such as CNTs and graphene.[23–28] The conducting pathways created by CNTs and graphene enable fast charge transfer in electrode/electrolyte interface due to their excellent electrical conductivity and large surface area. Among various phases of cobalt sulphide (CoS, Co_9S_8 and CoS_2), most reports in the literature demonstrate the use of only CoS-MWCNT composite for application in supercapacitor electrode. [23–25] But with Co_9S_8-MWCNT and

CoS_2-MWCNT, we could only get literature showing use in oxygen evolution reactions, photovoltaics, and batteries.[23–33] To the best of our knowledge there are no reports showing the use of CoS_2/MWCNT composite as supercapacitor electrode. Also, previous reports using CoS/MWCNT electrodes did not show any systematic investigation of the influence of CNTs on the electrochemical performance; rather what they reported is merely the synthesis and electrochemical properties of CoS/MWCNT composite thus leaving scope for further studies.

In view of the above, here we report a novel hydrothermal method for the synthesis of CoS_2-MWCNT nanohybrids for application as supercapacitor electrodes. The method is simple, cost-effective and scalable. This is also the first instance of a systematic investigation of the influence of MWCNTs on the electrochemical properties of CoS_2 nanoparticles. Several samples were prepared by varying the relative concentration of multiwalled CNT (MWCNT) in the nanohybrids to optimise the electrode performance. The microstructure and composition of these electrodes were initially characterized using electron microscopy, x-ray diffraction (XRD) and energy dispersive X-ray spectroscopy (EDX) and the specific surface area was investigated by Brunauer-Emmett-Teller (BET) adsorption isotherms. Electrochemical measurements were carried out to evaluate their suitability as electrode material for supercapacitor and the results revealed that the synthesized CoS_2-MWCNT nanohybrids have huge potential as future supercapacitor electrode material.

2. Experimental

2.1. Chemicals and Reagents

MWCNTs with 10-20 nm outer diameter, 10-30 μm length and 95% purity were purchased from Nanostructured & Amorphous Materials, Inc, Houston, USA. Cobalt nitrate hexahydrate ($Co(NO_3)_2$,$6H_2O$), l-cysteine, ethylene glycol, nafion, nitric acid (HNO_3), sodium hydroxide (NaOH), isopropyl alcohol (IPA) were all purchased from Sigma Aldrich and all chemicals except MWCNTs were used as received without any further purification.

2.2. Treatment of MWCNT

MWCNTs (1.5 gm) were refluxed in concentrated HNO_3 (150 ml) at 140°C for 12 hours. This acid treatment is expected to introduce –COOH bonds to the walls of MWCNTs which in turn can enhance its chemical reactivity as well as remove amorphous carbon and residual inorganic impurities.[34] After refluxing the reaction mixture was washed several times with deionized water until the pH value reached 7 and the MWCNTs were collected by filtering

through a Whatman filter paper. Finally the acid treated MWCNTs were dried in a vacuum oven at 60°C for overnight.

2.2. Synthesis of CoS_2-MWCNT Nanohybrids

Synthesis of the CoS_2-MWCNT nanohybrids was carried out by, first, suspending specific amounts of MWCNT in deionized water (40 ml) under ultrasonication for 30 minutes. Then the reaction mixture was placed in a magnetic stirrer at 500 rpm for a further 20 minutes. Then $Co(NO_3)_2,6H_2O$ (20 mM) was added to the reactant mixture under stirring. After 30 minutes 15 ml ethylene glycol was added slowly to the reaction vessel under vigorous stirring. After 15 minutes freshly prepared aqueous solution (40ml) of L-cysteine (3mg/ml) was added to the reaction mixture (Fig. 1). The reaction mixture was kept under stirring for another 1 hour and then transferred to a teflon lined stainless steel autoclave and heated in an oven at 150°C for 18 hours after which the autoclave was cooled normally to room temperature. The precipitate was washed several times with deionized water and ethanol before drying in a vacuum oven at 60 °C for 12 hours. Four different nanohybrid samples were prepared by changing the starting weight of the MWCNT: CoS_2-MWCNT(1) containing 10 wt% MWCNT, CoS_2-MWCNT(2) containing 15 wt% MWCNT, CoS_2-MWCNT(3) containing 20 wt% MWCNT, and CoS_2-MWCNT(4) containing 25 wt% MWCNT. The bare cobalt sulphide control sample was also synthesized by the same route without the addition of the MWCNTs.

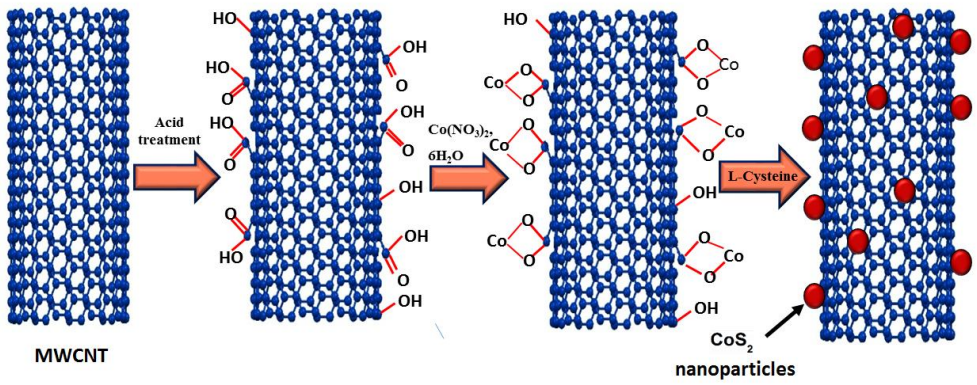

Fig. 1: Schematic diagram showing the synthesis of the CoS_2-MWCNT nanocomposite. For simplicity only one wall of the MWCNT is shown.

2.3. Material Characterization

X-ray diffraction (XRD) study of the synthesized powdered samples was carried out using a Philips Panalytical Xpert Pro diffractometer irradiated by a Cu Kα x-ray source (λ = 1.54 Å) at room temperature. Electron micrographs were recorded using a Carl Zeiss Sigma scanning electron microscope (FESEM) equipped with a field emission gun and operated at 5 kV. High resolution transmission electron microscopy (HRTEM) images were recorded on a JEOL-JEM 2100 transmission microscope operated at an accelerating voltage of 200 kV. The HRTEM samples were prepared by drop casting a homogeneous suspension of the samples on a carbon coated copper grid (300 mesh) and allowing it to dry in air. Elemental analysis was performed using an energy dispersive X-ray (EDX) spectroscope (Oxford Instruments) attached with the HRTEM. The specific surface areas of the samples were measured from the BET adsorption/desorption isotherms for nitrogen recorded using a BET surface analyser (Nova) supplied by Quantachrome Instruments, USA.

Electrochemical analysis of the nanohybrid electrodes were carried out in a three electrode cell containing a glassy carbon working electrode, Ag/AgCl reference electrode and a Pt wire as counter electrode. Measurements were made using an electrochemical workstation (CH660E by CH Instruments, USA) typically operated within a voltage window of 0.0V to +1.0V. To prepare the working electrode, first an IPA solution was made by dissolving nafion (500 mg/l) of which 25 µl was collected in a vial in which 5 mg of the as-synthesized nanohybrid sample was added before sonicating for ten minutes. 5 µl of this solution was then deposited on the pre-polished glassy carbon electrode (3 mm dia) and dried in air at room temperature. All three electrodes were immersed in 1M NaOH solution for all electrochemical analyses such as cyclic voltammetry (CV), galvanostatic charge discharge (GCD) and electrochemical impedance spectroscopy (EIS).

3. Results and Discussion

3.1. Structural and morphological analysis

The XRD plots of MWCNT, bare CoS_2 and CoS_2-MWCNT nanohybrids are shown in Fig. 2. The plot for bare cobalt sulphide shows several peaks indicating presence of mixed phases of CoS_2 and Co_9S_8. The peaks at 2θ value 27.5°, 32.3°,36.2°, 40.1°,46.4°, 54.9° represent reflections from (111), (002), (021), (112), (022) and (113) planes of cubic CoS_2 nano-crystals, respectively according to amcsd file no. 98-004-1934 with lattice parameter 5.39Å. The peaks at 2θ = 28.03°, 47.78° and 52.56° originate from the (311), (511) and (440) planes

of the hexagonal Co_9S_8 structure, respectively (amcsd file no. 000-5105). Cobalt sulphide is known to exist in a variety of stoichiometry resulting in a number of sulphides and *hence hereafter we shall denote this mixed phase of cobalt sulphide as* Co_xS_y. Interestingly, the XRD plot of the CoS_2-MWCNT nanohybrid shows peaks corresponding to cubic CoS_2 structure suggesting MWCNTs' strong influence to promote the growth of CoS_2 phase only while preventing formation of all other sulphides (CoS, Co_9S_8).

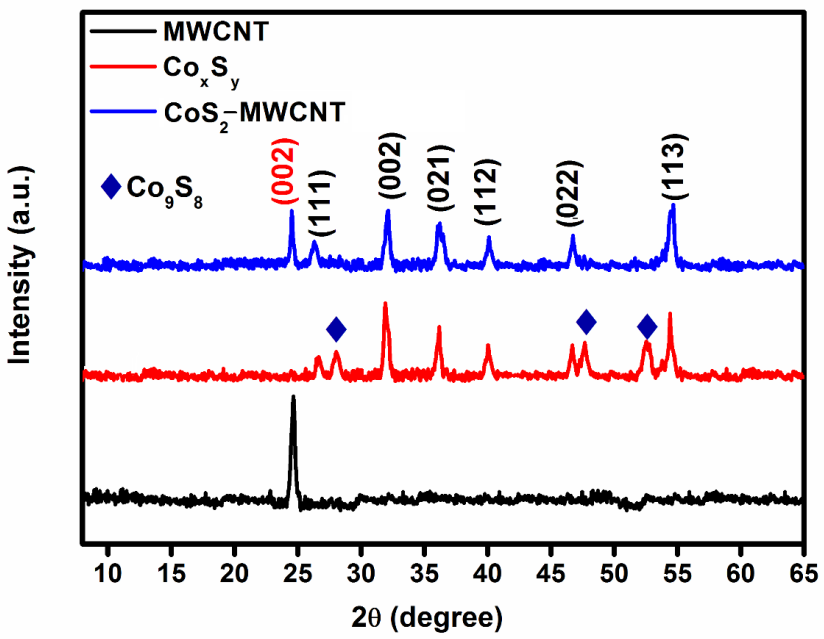

Fig. 2. X-ray diffractograms of MWCNT, bare Co_xS_y and CoS_2-MWCNT nanohybrids.

Fig. 2 also shows the characteristic diffraction peak of (002) plane of MWCNT in both pristine MWCNT and CoS_2-MWCNT nanohybrid samples. The intense and sharp diffraction peaks of cobalt disulphide indicate good crystallinity of CoS_2. The average crystallite size of CoS_2 in the CoS_2-MWCNT nanohybrid was calculated by *Debye-Scherer* equation,

$$d = n\lambda/\beta cos\,\theta \qquad (1)$$

where d = average crystallite size, n= 0.9, λ= wavelength of the Cu K_α source (1.54Å), β= full width at half maximum (FWHM) of the most intense peak in radian, 2θ is the = position of the most intense peak. The average crystallite size of CoS_2–MWCNT as obtained from equation (1) taking the most intense peak ($2\theta = 32.3°$) into account is found to be 12 nm.

A typical FESEM image (Fig. 3) shows the presence of uniformly distributed CoS_2 nanoparticles well attached on the surfaces of the MWCNTs for the CoS_2-MWCNT nanohybrid sample. The acid-treated MWCNTs possess some oxygen containing functional groups which serve as the host sites for the attachment of Co^{4+} ions (CoS_2 nanoparticles) due to electrostatic attraction between Co^{4+} and negatively polarized oxygen groups. Elemental mapping data recorded on a random region of the sample shows presence of C, O, Co and S atoms over the entire area suggesting uniform distribution of these elements within the CoS_2-MWCNT sample in accordance with the uniformly distributed CoS_2 nanoparticles well attached on the MWCNT network.

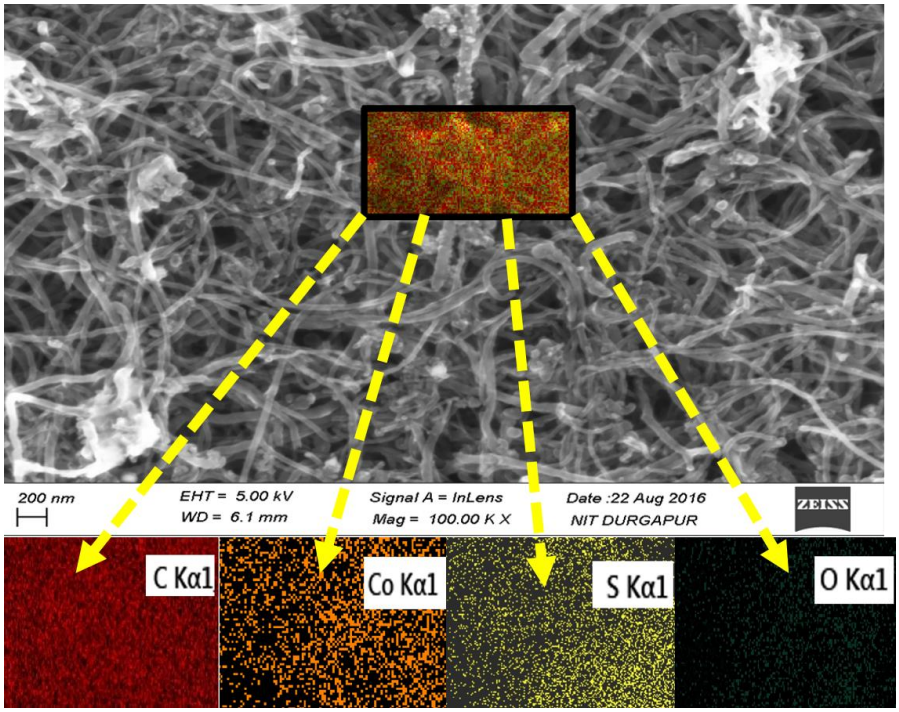

Fig. 3. FESEM image of CoS_2-MWCNT(3) nanohybrid along with the elemental mapping data corresponding to a random area of the sample.

The HRTEM image of CoS_2-MWCNT nanohybrid in Fig. 4(a) shows the presence of CoS_2 nanoparticles well attached to MWCNT walls, with no free CoS_2 particles visible. Fig. 4(b) depicts the particle size distribution of CoS_2 nanoparticles using ImageJ software and one can see that the mean diameter of the particles is ~9 nm which is in good agreement with that measured from XRD (12 nm). The nanosized CoS_2 particles have large surface to volume ratio and thus can generate large number of electrocatalytically active sites on the conducting

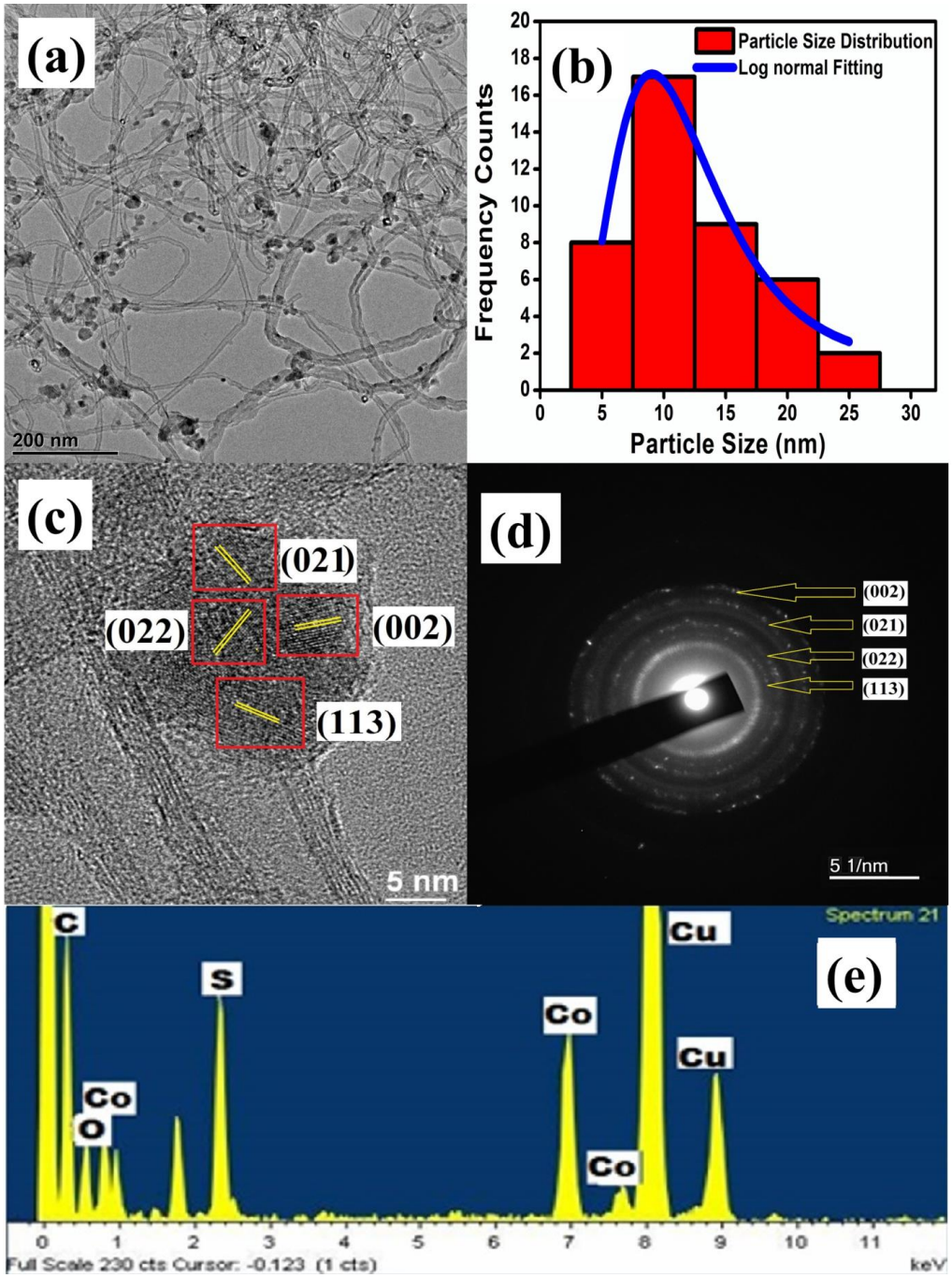

Fig. 4. (a) Typical HRTEM image, (b) size distribution of CoS_2 nanoparticles, (c) HRTEM image at higher magnification showing lattice fringes, (d) SAED pattern and (e) EDX spectrum of the CoS_2-MWCNT nanohybrid.

MWCNT network and is thus expected to improve the redox reaction kinetics for charge storage application. Fig. 4(c) demonstrates the presence of (021), (022), (002) and (113) planes of cubic CoS_2 with lattice spacing of 2.47Å, 1.96Å, 2.75Å and 1.66Å, respectively (amcsd file no. 98-004-1934). The rings present in the SAED pattern (Fig. 4(d)) show the polycrystalline nature of the CoS_2 nanoparticles and further confirms the presence of the same crystal planes of CoS_2 structure as in Fig. 4(c). The lattice resolved HRTEM image (4c) and SAED pattern (4d) also confirm that the cobalt sulphide present in the composite sample is CoS_2 phase only as lattice planes for other phases could not be identified.

Fig. 4(e) shows a representative EDX spectrum obtained from the image in Fig 4(a) which clearly shows presence of sharp and strong peaks corresponding to C, Cu, Co, and S. The spectrum also shows a weak oxygen peak originating from the functional groups of MWCNTs whereas the strong copper peaks appear due to the copper grid in which the samples were desposited for imaging. The elemental signal averaged over several locations of the of CoS_2-MWCNT nanohybrid sample revealed the presence of carbon (45.19 at.%), oxygen (14.21 at.%), cobalt (14.72 at.%) and sulphur (25.87 at.%). Thus the elemental data confirms formation of cobalt disulphide with stoichiometry closest to CoS_2 (Co:S = 1:2) in accordance with our observations from XRD (Fig. 2).

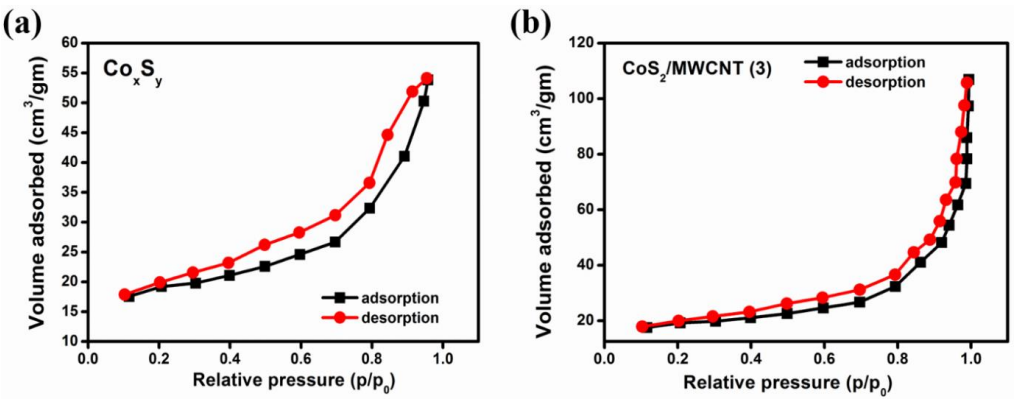

Fig. 5. N_2 adsorption-desorption isotherm of (a) Co_xS_y (b) CoS_2-MWCNT (3)

Since specific surface area of the electrode material is known to play an important role in its ability to store charge, the N_2 adsorption-desorption isotherms for bare Co_xS_y and the optimised CoS_2-MWCNT (3) nanohybrid sample were recorded for comparison which are shown in Fig. 5. The plot shows typical hysteresis loop in the larger range of relative pressure (P/P_0) illustrating that the nanohybrid has a typical mesoporous structure.[35] The specific

surface areas of the CoS_2-MWCNT (3) and bare Co_xS_y have been measured as 53.6 m^2/gm and 28.3 m^2/gm, respectively. The result is in good agreement with that of the FESEM image (Figure 4a) showing CoS_2 particles with average size of 10 nm in the nanohybrid sample compared to much larger (>100 nm) size nanopetals of the bare Co_xS_y sample (Supporting Information, Figure S1). Small particle size of CoS_2 and presence of MWCNT (with large surface area) results in overall increase of the surface area of the CoS_2/MWCNT nanohybrid sample compared to that of bare Co_xS_y. Increase in the surface area facilitates increase in the number of active catalysis sites available for reaction which in turn increases the specific capacitance of the nanohybrid due to enhanced charge storage.

3.2. Electrochemical Analysis

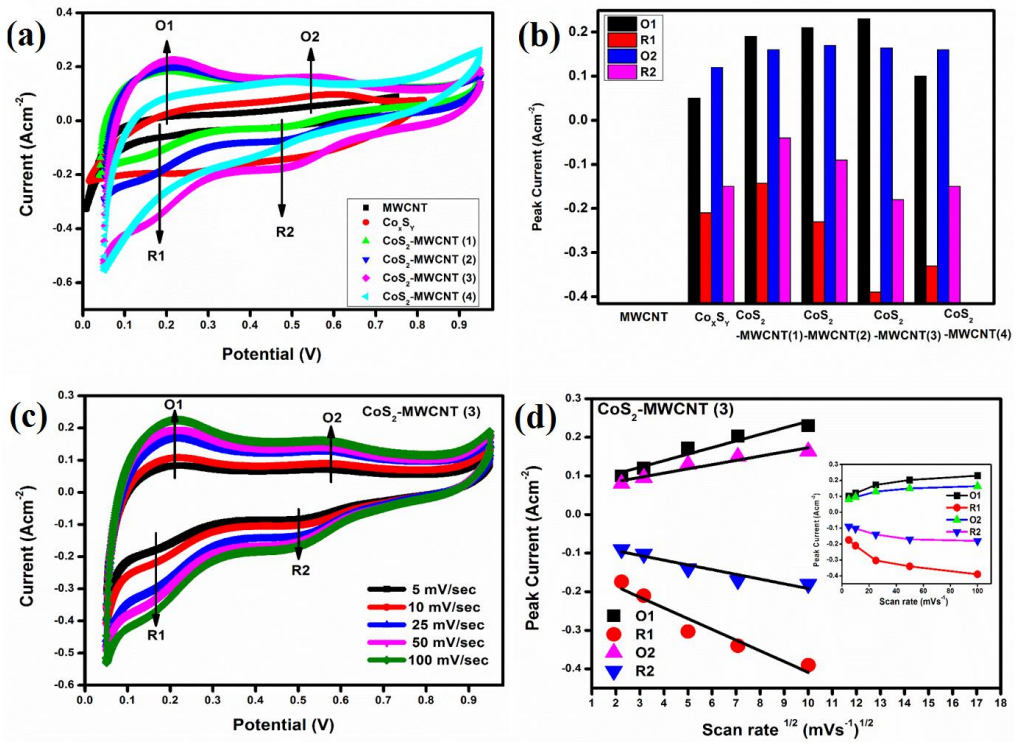

Fig. 6. (a) CV curves at scan rate of 100 mV/sec recorded with various CoS_2-MWCNT nanohybrid electrodes as well as with bare Co_xS_y and MWCNT, (b) histogram showing the redox peak current values, (c) CV curves of MWCNT-CoS_2(3) electrode at different scan rates, and (d) plot of redox peak currents for CoS_2-MWCNT(3) vs square root of scan rate and vs scan rate (inset).

The redox pair marked as R1 and O1 originates from reversible reaction between CoS_2 and CoS_2OH (Eq. 2) whereas that marked by R2 and O2 originates from the reaction between CoS_2OH and CoS_2O (Eq. 3) as shown in Fig. 6a, & 6b. The comparison of the CV curves recorded with MWCNT, Co_xS_y and CoS_2-MWCNT nanohybrids as electrode reveals that with increase in MWCNT weight fraction in the CoS_2-MWCNT nanohybrid the redox peak current values as well as the area under the CV curve increase (with the exception of CoS_2-MWCNT(4) sample) which can be attributed to the conductive pathways provided by the highly conducting MWCNT network. The peak current values for O1, R1, O2, R2 are separately plotted in Fig. 6b for a clear comparison where it is evident that the highest value of O1 and the lowest value of R1 are obtained for CoS_2-MWCNT(3) sample. MWCNT provides effective conductive channels for intercalation and de-intercalation of ions which in turn facilitates fast charge transfer in the electrode/electrolyte interface resulting in improved overall electrochemical performance.

$$CoS_2 + OH^- \leftrightarrow CoS_2OH + H_2O + e^- \quad \ldots\ldots\ldots\ldots\ldots\ldots\ldots\ldots\ldots\ldots\ldots\ldots\ldots\ldots (2)$$

$$CoS_2OH + OH^- \leftrightarrow CoS_2O + H_2O + e^- \quad \ldots\ldots\ldots\ldots\ldots\ldots\ldots\ldots\ldots\ldots\ldots\ldots\ldots\ldots (3)$$

However, Fig. 6 also shows that addition of MWCNT above a certain weight fraction (20% in this work), does not cause further improvement in the electrode performance as the peak current values deteriorate in the case of CoS_2-MWCNT(4) sample from the values recorded for all other CoS_2-MWCNT nanohybrid samples. Possible reason for this could be formation of agglomerates of MWCNTs which may hinder the fast charge diffusion. Another possible reason could be due to the reduction in the pseudocapacitance caused by the lowering of the CoS_2 fraction. This is also evident from Fig. 6a where redox pairs are not prominently visible for CoS_2-MWCNT(4) and the peak current values are significantly reduced. A closer look at the CV curve of the pristine MWCNT reveals a rectangular shape with absence of any prominent redox peaks in accordance with the EDLC behaviour of carbon materials. This behaviour is observed even when the scan rate is varied from 5 mV/s to 100 mV/s as shown in the Supporting Information (Fig. S2). On the other hand, bare Co_xS_y exhibits two prominent redox pairs but very low peak current values at all scan rates presumably due to its poor electrical conductivity which can also be seen in the Supporting Information (Fig. S3).

Among the whole set of CoS_2-MWCNT nanohybrids CoS_2-MWCNT(3) exhibits the best electrochemical behaviour with highest redox peak currents (Fig. 6b) and hence this sample

was further explored against varying scan rate (Fig. 6c). The curves show symmetric shape at all scan rates which indicating good reversibility and high rate performance.[22] The positions of the oxidation and reduction peaks of CoS_2-MWCNT(3) are slightly shifted to more positive and negative potential, respectively with increasing scan rate (Fig. 6c). This may result from the inability of ion diffusion process to achieve neutralization during faradaic redox reactions.[35–36] Other CoS_2-MWCNT nanohybrids also show similar CV curves as those of CoS_2-MWCNT(3) at varying scan rates which are shown in Supporting Information (Fig. S4, S5, S6). Fig. 6(d) shows plot of the oxidation and reduction peak currents recorded for CoS_2-MWCNT(3) sample against the scan rate and its square root. While the peak currents show a nonlinear relationship (inset in Fig. 6d) with scan rates, they exhibit an almost linear relationship with the square root of scan rate indicating a diffusion controlled redox reaction in the latter in accordance with the Randles-Sevcik equation [37] as given below:

$$i_p = 2.69 \times 10^5 n^{3/2} A D_0^{1/2} V^{1/2} C_0 \qquad (4)$$

where i_p represents the peak current, n is the no. of electrons transferred, A is the active surface area of the electrode, D_0 is diffusion coefficient of the rate limiting protons, V is the scan rate and C_0 is the concentration of protons. On the other hand, for an adsorption controlled process the relation between peak current and scan rate should be linear which is not what we see in the inset of Fig. 6d.[38] Thus, it is evident that the charge transfer kinetics is controlled by diffusion rather than adsorption.

GCD measurements were carried out from 0.0 V to 0.9 V at 1 A/gm current density (Fig. 7a) to further evaluate the potential of CoS_2-MWCNT nanohybrid as supercapacitor electrode. It can be seen that with increasing MWCNT weight fraction in CoS_2-MWCNT nanohybrid the charge-discharge response improves only upto 20% MWCNT fraction above which the electrochemical performance of the nanohybrid got reduced. In addition to providing fast charge diffusion channels, MWCNT also restricts the agglomeration of CoS_2 nanoparticles which synergistically contribute to improve the overall electrochemical response of the nanohybrid. However, for MWCNT weight fraction over and above 20% as in CoS_2-MWCNT(4) sample, a reduction in the GCD response occurs probably due to aggregation of MWCNTs and reduction of electrocatalytically active sites (less CoS_2 particles) on the electrode which in turn leads to an increase in the charge transfer resistance and lowers the specific capacitance.

The specific capacitance of the synthesized nanohybrid electrode was calculated from the GCD curves as in Fig. 6a using the following equation:

$$C_m = I \times \Delta t/(m \times \Delta V) \quad (5)$$

where C_m is the specific capacitance in Farad/gram (F/g), I is the discharge current in Ampere (A), Δt is the time elapsed for discharging in sec.(s), m is the mass of the active material in g, ΔV is the change of potential during discharging in Volt (V).

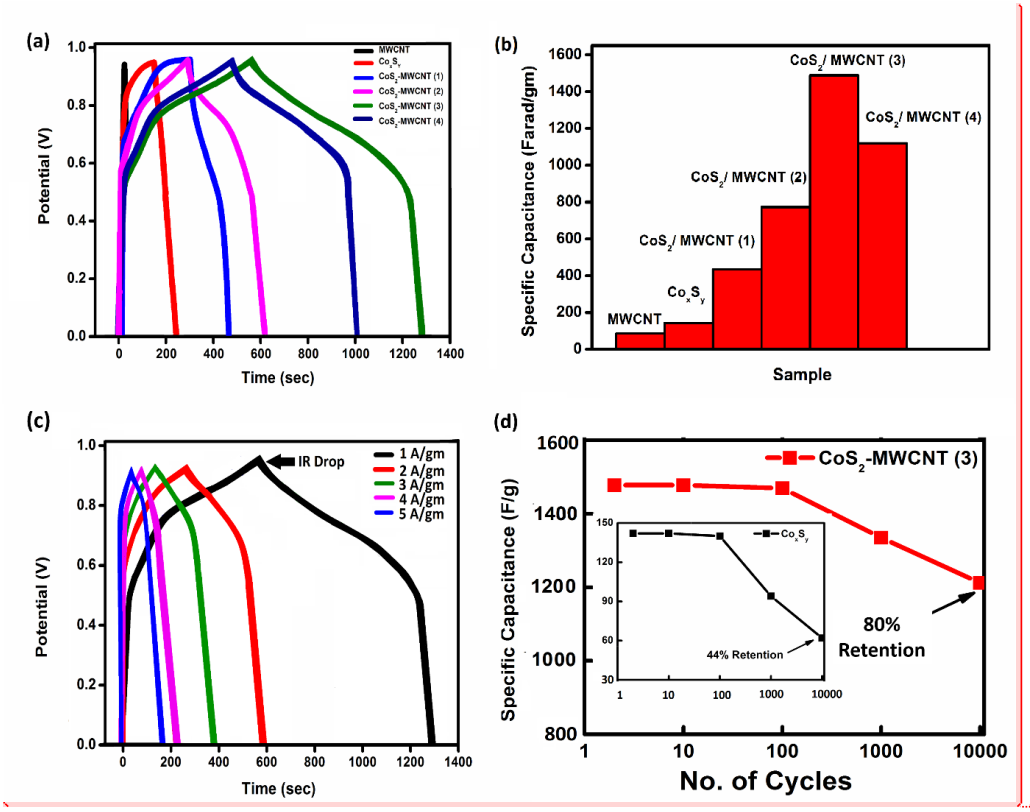

Fig. 7. (a) GCD curves recorded with current density of 1 A/g for various electrodes, (b) histogram plot of the calculated specific capacitance values for different electrodes, (c) GCD curves of CoS_2-MWCNT(3) electrode at different current densities and (d) Cycling ability of the CoS_2-MWCNT(3) and bare Co_xS_y electrodes at 1 A/gm current density.

The calculated values of the specific capacitance for all the samples using equation (4) are plotted as a histogram in Fig. 7(b). Among the synthesized set of nanohybrids CoS_2-MWCNT(3) exhibits the highest specific capacitance value of 1486 F/g at 1 A/gm current density which is almost 17 times and 11 times higher than that of MWCNT and bare Co_xS_y,

Comment [U1]: Replace

respectively. The synergistic effect of conducting MWCNT and highly catalytic CoS_2 results in such high capacitance value and improved electrochemical response. It can also be seen that CoS_2-MWCNT(4) exhibits lower specific capacitance value of 1120 F/gm compared to that for CoS_2-MWCNT(3) sample which is in good agreement with our previous CV results. Further, GCD response of CoS_2-MWCNT(3) at different current densities ranging from 1A /gm to 5 A/gm are shown in Fig. 7c which shows a monotonous decrease in the charging and discharging time as expected. The GCD curves are very much symmetric in nature showing good reversibility with increasing current density. There is a very low *IR* drop in the discharge curves which implies fast response and good charge transport at the electrode/electrolyte interface.[39]

For a supercapacitor, long cycle life being one of the major requirements, its electrode must possess long cycling ability and chemical stability. To evaluate the cycling stability of the electrode materials, we have run GCD measurements for 10,000 continuous cycles at 1 A/gm current density and calculated the specific capacitances at certain intervals the results of which are presented in Fig. 7d. It is evident that even after 10,000 cycles CoS_2-MWCNT(3) retains 80% of its initial specific capacitance value compared to only 44% retention for bare Co_xS_y electrode indicating the former's superior stability. The increased stability of the composite electrode is a direct consequence of the incorporation of MWCNTs due to their excellent, chemical and mechanical stability.[40] The relatively small (20%) loss in the specific capacitance value observed after 10,000 cycles is not surprising given the possibility of formation of localised aggregates as well as detachment of some CoS_2 nanoparticles from the MWCNT network due to prolonged exposure of the film in liquid electrolyte.

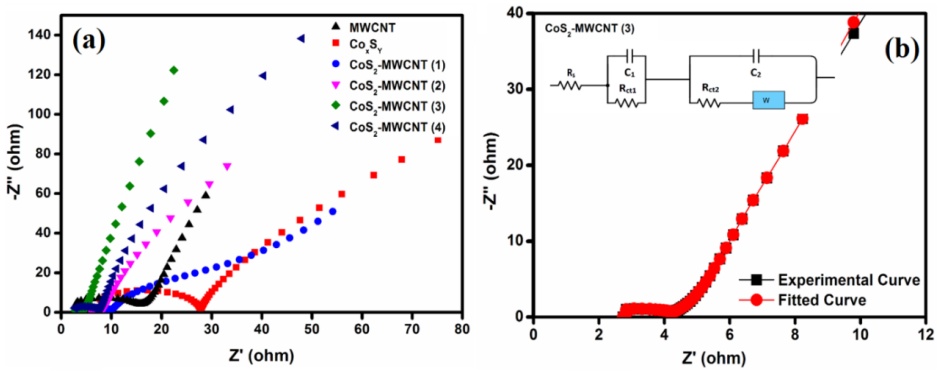

Fig. 8. (a) EIS curves of CoS_2-MWCNT nanohybrids, bare Co_xS_y and MWCNT. (b) Experimental and fitted EIS plot of CoS_2-MWCNT(3), and the equivalent electrical circuit.

EIS is one of the principal methods used to investigate the charge transfer mechanisms at electrode/electrolyte interface. EIS measurements were carried out on all samples in the frequency range of 10^5 Hz to 0.01 Hz. Nyquist plots of the nanohybrids, bare MWCNT and bare Co_xS_y all show semicircular curve in the high frequency region and a rising straight line in the lower frequency region (Fig. 8a). The intercepts of the semicircle with real impedance axis in higher frequency region indicate bulk resistance (R_s) of the electrochemical system which comprises of total resistance of the working electrode, solution resistance and resistance at electrode/electrolyte interface. The diameter of the semicircle is associated with the charge transfer resistance (R_{ct}) and the rising straight line at low frequency region stands for Warburg impedance. Generally, a steeper slope indicates a better pseudocapacitive behaviour. For better understanding, the magnified views of the semicircular region of the curves in high frequency region are given in the Supporting information (Fig. S7). The R_s and R_{ct} values of different nanohybrids, MWCNT and bare Co_xS_y are listed in Table 1.

Table 1: Different resistance values for various samples as obtained from the Nyquist plots.

Electrode Material	R_s (ohm)	R_{ct} (ohm)
MWCNT	2.79	15.52
Co_xS_y	7.73	20.89
CoS_2-MWCNT (1)	6.68	10.06
CoS_2-MWCNT (2)	6.01	8.02
CoS_2-MWCNT (3)	2.74	4.27
CoS_2-MWCNT (4)	2.76	7.35

It is evident from the above table that bare Co_xS_y has the highest R_s and R_{ct} suggesting its poor charge transfer properties as expected due to its poor electrical conductivity. The synergistic effect of MWCNT and CoS_2 gradually improves the ion diffusion mechanism which is evident from the lowering of the values of resistances from CoS_2-MWCNT(1) to CoS_2-MWCNT(3). Again, amongst all samples tested, CoS_2-MWCNT(3) exhibits the lowest bulk resistance and charge transfer resistance which signifies fastest charge transfer mechanism. Also the nearly vertical curve at low frequency region implies excellent pseudocapacitive behaviour of CoS_2-MWCNT(3). The equivalent circuit of the Nyquist plot of CoS_2-MWCNT(3) is shown in the inset of Fig. 8b. R_s is in series with double layer capacitance (C_1) and faradaic pseudo capacitance (C_2). W represents the Warburg impedance

and R_{ict} and R_{ect} denote charge transfer resistance in electrode/electrolyte interface and electron transfer resistance of the redox reactions, respectively. In case of CoS_2-MWCNT(4) the resistances increased slightly from those of CoS_2-MWCNT(3) in line with our findings of CV and GCD.

Based on the above results and previous knowledge of the properties of MWCNT, the main features of the nanohybrid that are responsible for its improved electrochemical performance can be summarized as below:

i) formation of a conducting network of MWCNTs results in faster charge transport that leads to lowering of the charge transfer resistance.

ii) large surface area of MWCNTs results in an overall increase in the active area of the electrode making more catalytic reaction to occur.

iii) high chemical and mechanical stability of MWCNT provides robustness to the electrode which in turn helps improving the cycle stability of the nanohybrid electrode.

iv) relatively low molarity of the electrolyte used in this work (1M NaOH) ensures less corrosion of the electrode leading to high cycling stability.

Table 2: Specific capacitance and cycle stability data for various cobalt sulphide based electrodes

Electrode Material	Name of the Electrolyte	Electro-lyte molarity	Current Density (A/gm)	No. of Cycles (N)	Initial value of Specific Capacitance (F/gm)	Specific Capacitance after N cycles (F/gm)	% retention of specific capacitance after N cycles
Co_9S_8 nanotubes[14]	KOH	6M	0.5	1000	285	246.5	86.5%
$Co_{1-x}S$ nanoflower[15]	KOH	2M	5	1000	666	548	81%
CoS@rGO[41]	KOH	2M	1	3000	849	768.4	90.5%
CoS_x [42]	KOH	6M	5	100	475	432.3	91%
CoS_2/MWCNT(3) This work	NaOH	1M	1	10,000	1486	1188	80%

In order for the reader to understand the significance of this work with respect to other published work on cobalt sulphide based electrode, the main electrochemical parameters as measured by other groups and in this article have been compared in table 2. The data in table 2 clearly establishes CoS_2-MWCNT(3) hybrid prepared in this work as the best electrode

material amongst similar materials reported by others for a number of reasons as follows. First, the specific capacitance value obtained in this work is much higher than previous reports. Second, most of the previous researchers measured the specific capacitance in strong alkaline electrolyte (6M KOH) which often leads to corrosion of the electrode leading to poor stability. In the present work, the measurements were performed at relatively weak medium (1 M NaOH) to improve stability. Last but not the least, the cycle stability of the electrode materials listed in table 2 shows very high cycle stability of the CoS2/MWCNT(3) electrode synthesized in this work even after 10,000 cycles compared to only a couple of thousands cycles for the similar materials synthesized by other groups. Most of these reports only showed cyclic stability data for upto 1000 cycles only which raises some doubts over the stability of these materials at 10,000 cycles. As cycling stability is one of the most significant parameters for a good electrode material for supercapacitor, the best stability was obtained by X et al[42] in which 90% charge was retained after 3000 cycles whereas all other works reported stability data for only 1000 cycles. However, commercial supercapacitors are expected to have very long cycle stability as the charge retention continues to drop even after thousands of charge-discharge cycles and this separates the present work from previous reports as we show upto 80% charge retention even after 10,000 cycles. This can be further understood from Figure 7(d) which shows a significant loss of specific capacitance value after 1000 cycles thus suggesting the importance of performing charge-discharge tests beyond 1000 cycles.

4. Conclusions

In summary, we show novel hydrothermal method to synthesise CoS_2 nanoparticle (9 nm mean diameter) decorated MWCNT nanohybrids for application in supercapacitor electrode. Incorporation of MWCNT promotes growth of cobalt sulphide with CoS_2 stoichiometry only and restricts the formation of all other stoichiometries such as CoS, Co_9S_8 etc. The electrochemical studies show that the synergistic effect due to high conductivity and large surface area of MWCNT and high catalytic activity of CoS_2 leads to increase in the redox reaction and faster charge transfer processes compared to those of bare MWCNT and bare cobalt sulphide. This study also reveals the existence of an optimum weight fraction of MWCNT (20 wt%) for which the specific capacitance attains its highest value which decreases upon both increase and decrease of MWCNT fraction. The CoS_2-MWCNT(3) sample containing optimized weight fraction of MWCNT exhibits specific capacitance of ~1486 F/gm at 1 A/gm current density which is much better than many previous reports on

similar electrode material. Further, the nanohybrid electrode showed excellent cycle stability with 80% retention of specific capacitance even after 10,000 cycles which is remarkable for potential application.

The improved electrochemical charge storage with the optimized CoS_2-MWCNT(3) electrode is a direct consequence of the incorporation of highly conducting MWCNTs which form a conducting network for faster charge transport between the catalytically active CoS_2 nanoparticles. Further, the extremely high chemical and mechanical stability of MWCNT ensures exceptionally high cyclic stability. The results shown in this article establishes CoS_2-MWCNT(3) sample as a very promising electrode material for supercapacitor.

Supporting Information

The Supporting Information is available free of charge on the ACS Publications website at DOI:….

FESEM image of bare Co_xS_y, CV curves of bare MWCNT, bare Co_xS_y, and the three different CoS_2/MWCNT composites (unoptimised) at various scan rates, and expanded EIS plot of the high frequency region.

Acknowledgements

The authors acknowledge the MHRD, Govt. of India for the "Centre of Excellence in Advanced Materials" grant of April 2013 under the Technical Education Quality Improvement Programme (TEQIP) phase II for funding this research.

References

[1] Simon, P.; Gogotsi,Y. Materials for Electrochemical Capacitors. *Nat. Mater.* **2008**, *7*, 845–854.

[2] Vijayakumar, S.; Nagamuthu, S.; Muralidharan, G. Supercapacitor studies on NiO Nanoflakes Synthesized through a Microwave Route. *ACS Appl. Mater. Interfaces* **2013**, *5*, 2188–2196.

[3] Zhang, L.L.; Zhao, X.S. Carbon-based Materials as Supercapacitor Electrodes. *Chem. Soc. Rev.* **2009**, *38*, 2520–2531.

[4] Yu, Z.; Tetard, L.; Zhai, L.; Thomas, J. Supercapacitor Electrode Materials: Nanostructures from 0 to 3 Dimensions. *Energy Environ. Sci.* **2015**, *8* , 702–730.

[5] Huang, M.; Li, F.; Dong, F.; Zhang, Y.X.; Zhang, L.L. MnO_2 -Based Nanostructures for High-Performance Supercapacitors. *J. Mater. Chem. A* **2015**, *3* , 21380–21423.

[6] Nithya, V.D.; Arul, N.S. Review on α-Fe_2O_3 based Negative Electrode for High Performance Supercapacitors. *J. Power Sources* **2016** , *327*, 297–318.

[7] Tummala, R.; Guduru, R.K.; Mohanty, P.S. Nanostructured Co_3O_4 Electrodes for Supercapacitor Applications from Plasma Spray Technique. *J. Power Sources* **2012** , *209*,44–51.

[8] Khosrozadeh, A.; Darabi, M.A.; Xing,M.; Wang,Q. Flexible Electrode Design: Fabrication of Freestanding Polyaniline-Based Composite Films for High-Performance Supercapacitors. *ACS Appl. Mater. Interfaces* **2016** , *8* , 11379–11389.

[9] Wang, H.; Song, Y.; Zhou, J.; Xu, X.; Hong, W.; Yan, J.; Xue, R.; Zhao, H.; Liu, Y.; Gao, J. High-Performance Supercapacitor Materials Based on Polypyrrole Composites Embedded with Core-Sheath Polypyrrole@$MnMoO_4$ Nanorods. *Electrochim. Acta.* **2016**, *212* , 775–783.

[10] Chen, T.; Dai, L. Carbon Nanomaterials for High-Performance Supercapacitors. *Materials Today* **2013** , *16* , 272–280.

[11] *Carbon Nanotubes: Synthesis, Structure, Properties, and Applications*; Dresselhaus, M.S., Dresselhaus, G., Avouris, G.P. ; Springer , 2001.

[12] Zhu, Y.; Murali, S.; Cai, W.; Li, X.; Suk, J.W.; Potts, J.R.; Ruoff, R.S. Graphene and Graphene Oxide: Synthesis, Properties, and Applications. *Adv. Mater.* **2010** , *22* , 3906–3924.

[13] Yu, G.; Hu, L.; Liu, L.; Wang, N.H.; Vosgueritchian, M.; Yang, Y. Enhancing the Supercapacitor Performance of Graphene / MnO_2 Nanostructured Electrodes by Conductive Wrapping. *Nano Lett.* **2011**, *11* , 4438–4442.

[14] Meriga, V.; Valligatla, S.; Sundaresan, S.; Cahill, C.; Dhanak, V.R.; Chakraborty, A.K. Optical, Electrical, and Electrochemical Properties of Graphene Based Water Soluble Polyaniline Composites. *J. Appl. Polym. Sci.* **2015**, *132*, 1–9.

[15] Agrawalla, R.K.; Paul, R.; Sahoo, P.K.; Chakraborty, A.K.; Mitra, A.K. Solvothermal Synthesis of a Polyaniline Nanocomposite- A Prospective Biosensor Electrode Material. *Express Polymer Letters* **2016**, *10* ,780–787.

[16] Trung, N.B.; Van Tam, T.; Dang, D.K.; Babu, K.F.; Kim, E.J.; Kim, J.; Choi, W.M.; Facile Synthesis of Three-Dimensional Graphene/Nickel Oxide Nanoparticles Composites for High Performance Supercapacitor Electrodes. *Chem. Eng. J.* **2015**, *264*, 603–609.

[17] Agrawalla, R.K.; Paul, S.; Sahoo, P.K.; Chakraborty, A.K.; Mitra, A.K. A Facile Synthesis of a Novel Three-Phase Nanocomposite: Single-wall Carbon Nanotube/Silver Nanohybrid Fibers Embedded in Sulfonated Polyaniline. *J. Appl. Polym. Sci.* **2015**, *132*, 1–9.

[18] Park, J.H.; Ko, J.M.; Park, O.O.; Kim, D.W. Capacitance Properties of Graphite/Polypyrrole Composite Electrode Prepared by Chemical Polymerization of Pyrrole on Graphite Fiber. *J. Power Sources* **2002**, *105* , 20–25.

[19] Gao, Z.; Yang, W.; Wang, J.; Wang, B.; Li, Z.; Liu, Q.; Zhang, M.; Liu, L. A New Partially Reduced Graphene Oxide Nanosheet / Polyaniline Nanowafer Hybrid as Supercapacitor Electrode Material. *Energy Fuels* **2013**, *27*, 568–575.

[20] Rui, X.; Tan, H.; Yan, Q. Nanostructured Metal Sulfides for Energy Storage. *Nanoscale* **2014**, *6*, 9889–9924.

[21] Wan, H.; Ji, X.; Jiang, J.; Yu, J.; Miao, L.; Zhang, L.; Bie, S.; Chen, H.; Ruan,Y. Hydrothermal Synthesis of Cobalt Sulfide Nanotubes: The Size Control and its Application in Supercapacitors. *J. Power Sources* **2013**, *243*, 396–402.

[22] Li, Y.; Liu, S.; Chen, W.; Li, S.; Shi, L.; Zhao, Y. Facile Synthesis of Flower-Like Cobalt Sulfide Hierarchitectures with Superior Electrode Performance for Supercapacitors. *J. Alloys Compd.* **2017**, *712*, 139–146.

[23] Chen, C.Y.; Shih, Z.Y.; Yang, Z.; Chang, H.T. Carbon Nanotubes/Cobalt Sulfide Composites as Potential High-Rate and High-Efficiency Supercapacitors. *J. Power Sources* **2012**, *215*, 43–47.

[24] Dai, K.; Lv, J.; Lu, L.; Liang, C.; Geng, L.; Zhu, G. Large-Scale Synthesis of Cobalt Sulfide/Carbon Nanotube Hybrid and its Excellent Electrochemical Capacitance Performance. *Materials Letters* **2016**, *176* , 42–45.

[25] Lin, J.Y.; Tai, S.Y.; Chou, S.W. Bifunctional One-Dimensional Hierarchical Nanostructures Composed of Cobalt Sulfide Nanoclusters on Carbon Nanotubes Backbone for Dye-Sensitized Solar Cells and Supercapacitors. *J. Phys. Chem. C* **2014**, *118*, 823–830.

[26] Qu, B.; Chen, Y.; Zhang, M.; Hu, L.; Lei, D.; Lu, B.; Li, Q.; Wang, Y.; Chen, L.;

Wang, T. B-Cobalt Sulfide Nanoparticles Decorated Graphene Composite Electrodes for High Capacity and Power Supercapacitors. *Nanoscale* **2012**, *4*, 7810–7816.

[27] Huang, G.; Chen, T.; Wang, Z.; Chang, K.; Chen, W. Synthesis and Electrochemical Performances of Cobalt Sulfides / Graphene Nanocomposite as Anode Material of Li-Ion Battery. *J. Power Sources* **2013**, *235*, 122–128.

[28] Xu, L.; Lu, Y. One-Step Synthesis of a Cobalt Sulfide/Reduced Graphene Oxide Composite Used as an Electrode Material for Supercapacitors. *RSC Adv*. **2015**, *5*, 67518–67523.

[29] Zhou, H.; Hu, J. Facile Synthesis of Multi-Walled Carbon Nanotubes/Co_9S_8 Composites with Enhanced Performances for Sodium-Ion Battery. *Materials Letters* **2017**, *195*, 26–30.

[30] Xie, S.; Deng, Y.; Mei, J.; Yang, Z.; Lau, W.M.; Liu, H. Facile Synthesis of CoS_2/CNT Composite and its Exploitation in Thermal Battery Fabrication. *Compos. Part B: Eng.* **2016**, *93*, 203–209.

[31] Zhang, X.; Liu, X.J.; Wang, G.; Wang, H. Cobalt Disulfide Nanoparticles/ Graphene/Carbon Nanotubes Aerogels with Superior Performance for Lithium and Sodium Storage. *J. Coll. Interf. Sci.* **2017**, *505*, 23–31.

[32] Tao, L.; Xianmin, M.; Haijun, C. Carbon Nanotube Aerogel-CoS_2 Hybrid Catalytic Counter Electrodes for Enhanced Photovoltaic Performance Dye-Sensitized Solar Cells. *Nanoscale* **2018**, *10*, 4194–4201.

[33] Jizhang, Y.; Zhi, Y.; Hua, L.L. Highly Efficient Oxygen Evolution from Cos_2/CNT Nanocomposites via a One-Step Electrochemical Deposition and Dissolution Method. *Nanoscale* **2017**, *9*, 6886–6894.

[34] Coleman, K.S.; Chakraborty, A.K.; Bailey, S.R.; Sloan, J.; Alexander, M. Iodination of Single-Walled Carbon Nanotubes. *Chem. Mater.* **2007**, *19*, 1076–1081.

[35] Chen, S.; Zhu, J.; Wu, X.; Han, Q.; Wang, X. Graphene Oxide-MnO_2 Nanocomposites for Supercapacitors. *ACS Nano* **2010**, *4*, 2822–2830.

[36] Wei, W.; Cui, X.; Chen, W.; Ivey, D.G. Electrochemical Cyclability Mechanism for MnO_2 Electrodes Utilized as Electrochemical Supercapacitors. *J. Power Sources* **2009**, *186*, 543–550.

[37] Sarkar, A.; Chakraborty, A.K.; Bera, S. NiS/rGO nanohybrid: An Excellent Counter Electrode for Dye Sensitized Solar Cell. *Sol. Energy Mater Sol. Cells.* **2018**, *182*, 314–320.

[38] Hu, Z.A.; Xie, Y.L.; Wang, Y.X. ; Xie, L.J.; Fu, G.R.; Jin, X.Q. ; Zhang, Z.Y.; Yang, H.Y.; Wu, Y.Y. Synthesis of rGO-Cobalt Hydroxides with Different Intercalated Anions and Effects of Intercalated Anions on Their Morphology, Basal Plane Spacing, and Capacitive Property. *J. Phys. Chem. C.* **2009**, *113*, 12502–12508.

[39] Wang, J.G. ; Zhou, R.; Jin, D.; Xie, K.; Wei, B. Controlled Synthesis of $NiCo_2S_4$ Nanostructures on Nickel Foams for High-Performance Supercapacitors. *Energy Storage Mater.* **2016**, *2*, 1–7.

[40] Chakraborty, A. K. ; Coleman, K. S. Poly(ethylene) glycol/Single-walled Carbon Nanotube Composites. *J. Nanosci. Nanotechnol.* **2008**, *8*, 4013–4016.

[41] Song, X.; Tan, L.; Wang, X.; Zhu, L; Yi, X.; Dong, Q. Synthesis of CoS@rGO Composites with Excellent Electrochemical Performance for Supercapacitors. *J. Electroana.l Chem.***2017**, *794*, 132–138.

[42] Tao, F.; Zhao, Y.Q.; Zhang, G.Q.; Li, H.L. Electrochemical Characterization on Cobalt Sulfide for Electrochemical Supercapacitors. *Electrochem. Commun.* **2007**, *9*, 1282–1287.